



University of
Zurich^{UZH}

Zurich Open Repository and
Archive

University of Zurich
University Library
Strickhofstrasse 39
CH-8057 Zurich
www.zora.uzh.ch

Year: 2023

Search for the rare decays $W \rightarrow D_s \gamma$ and $Z \rightarrow D \gamma$ at LHCb

LHCb Collaboration ; Bernet, R ; Müller, K ; Owen, P ; Serra, N ; Steinkamp, O ; et al

DOI: <https://doi.org/10.1088/1674-1137/aceae9>

Posted at the Zurich Open Repository and Archive, University of Zurich

ZORA URL: <https://doi.org/10.5167/uzh-253433>

Journal Article

Published Version



The following work is licensed under a Creative Commons: Attribution 3.0 Unported (CC BY 3.0) License.

Originally published at:

LHCb Collaboration; Bernet, R; Müller, K; Owen, P; Serra, N; Steinkamp, O; et al (2023). Search for the rare decays $W \rightarrow D_s \gamma$ and $Z \rightarrow D \gamma$ at LHCb. *Chinese Physics C*, 47(9):093002.

DOI: <https://doi.org/10.1088/1674-1137/aceae9>

PAPER • OPEN ACCESS

Search for the rare decays $W^+ \rightarrow D_s^+ \gamma$ and $Z \rightarrow D^0 \gamma$ at LHCb

To cite this article: LHCb Collaboration *et al* 2023 *Chinese Phys. C* **47** 093002

View the [article online](#) for updates and enhancements.

You may also like

- [Centrality determination in heavy-ion collisions with the LHCb detector](#)
R. Aaij, C. Abellán Beteta, T. Ackernley et al.
- [Beam test performance of a prototype module with Short Strip ASICs for the CMS HL-LHC tracker upgrade](#)
The Tracker Group of the CMS collaboration]Corresponding author: Marc Osherson., W. Adam, T. Bergauer et al.

Search for the rare decays $W^+ \rightarrow D_s^+ \gamma$ and $Z \rightarrow D^0 \gamma$ at LHCb

LHCb Collaboration[†]

Abstract: A search for the rare decays $W^+ \rightarrow D_s^+ \gamma$ and $Z \rightarrow D^0 \gamma$ is performed using proton-proton collision data collected by the LHCb experiment at a centre-of-mass energy of 13 TeV, corresponding to an integrated luminosity of 2.0 fb^{-1} . No significant signal is observed for either decay mode and upper limits on their branching fractions are set using $W^+ \rightarrow \mu^+ \nu$ and $Z \rightarrow \mu^+ \mu^-$ decays as normalization channels. The upper limits are 6.5×10^{-4} and 2.1×10^{-3} at 95% confidence level for the $W^+ \rightarrow D_s^+ \gamma$ and $Z \rightarrow D^0 \gamma$ decay modes, respectively. This is the first reported search for the $Z \rightarrow D^0 \gamma$ decay, while the upper limit on the $W^+ \rightarrow D_s^+ \gamma$ branching fraction improves upon the previous best limit.

Keywords: W/Z boson, rare decay, upper limit of branching fraction

DOI: 10.1088/1674-1137/aceae9

I. INTRODUCTION

The large production cross-sections of W and Z bosons at hadron colliders offer unique opportunities to search for their rare decays, which can be used to test the Standard Model (SM) and probe for physics beyond the SM. Particularly interesting are the radiative decays of the W and Z bosons, predictions of their branching fractions using the quantum chromodynamics (QCD) factorization [1–6] range from 10^{-6} to 10^{-12} . Unlike in B -meson decays, where large power corrections to the decay rates lead to sizable theoretical uncertainties, power corrections in W and Z boson decays are under good control due to the large energy released to the final state hadrons. Thus, the study of hadronic-radiative W and Z bosons decays can provide stringent tests of the QCD factorization formalism [5]. After almost forty years from the discoveries of the W and Z bosons, no hadronic-radiative decay of these bosons has been observed, despite searches performed by the ATLAS [7–11], CMS [12], and CDF [13] collaborations. The current best limit is 9×10^{-7} for the branching fraction of the $Z \rightarrow \phi \gamma$ decay [9].

This paper presents searches for the radiative decays $W^+ \rightarrow D_s^+ \gamma$ and $Z \rightarrow D^0 \gamma$, followed by $D_s^+ \rightarrow K^+ K^- \pi^+$ and $D^0 \rightarrow K^- \pi^+$, at the LHCb experiment, taking advantage of its excellent hadron identification capabilities.¹⁾

The radiative decay $W^+ \rightarrow D_s^+ \gamma$ can proceed via tree-level diagrams as shown in Fig. 1 and its branching fraction is predicted to be $(3.7 \pm 1.5) \times 10^{-8}$ in the SM [5]. A

previous search for this decay by the CDF collaboration found no significant signal and determined the limit $\mathcal{B}(W^+ \rightarrow D_s^+ \gamma) < 1.3 \times 10^{-3}$ at 95% confidence level [13].

The radiative decay $Z \rightarrow D^0 \gamma$ is a flavour-changing-neutral-current (FCNC) process, forbidden at the tree level, and can only proceed via higher-order loop processes in the SM, as shown in Fig. 2. The FCNC couplings of Z boson are heavily constrained by the existing precision measurements from flavour physics, resulting in a negligible branching fraction ($\mathcal{O} \sim 10^{-15}$) of $Z \rightarrow D^0 \gamma$ mode. However, a search for this decay can provide a model-independent way to probe the FCNC couplings of the Z boson [5]. To date, there is no experimental study of this process.

The search uses data from proton-proton collisions at 13 TeV collected by the LHCb experiment, corresponding to a luminosity of 2.0 fb^{-1} . These data were collected in 2018 when the trigger selection dedicated to these decays was implemented. Both relative and absolute branching fractions of the decays $W^+ \rightarrow D_s^+ \gamma$ and $Z \rightarrow D^0 \gamma$ are determined, using $W^+ \rightarrow \mu^+ \nu$ and $Z \rightarrow \mu^+ \mu^-$ decays as normalization channels, respectively. In this article, the fiducial criteria require that the particle lie within the LHCb acceptance, $10 < \theta < 400$ mrad for the charged particles, and $25 < \theta_x < 300$ mrad and $25 < \theta_y < 250$ mrad for the neutral particles, where θ is the polar angle with respect to the beam direction and $\theta_{x(y)}$ is the projection of the polar angle on the xz (yz) plane.

Received 15 December 2022; Accepted 5 July 2023; Published online 7 August 2023

[†] Authors are listed at the end of this paper.

1) The inclusion of charge-conjugate processes is implied throughout.



Content from this work may be used under the terms of the Creative Commons Attribution 3.0 licence. Any further distribution of this work must maintain attribution to the author(s) and the title of the work, journal citation and DOI. Article funded by SCOAP³ and published under licence by Chinese Physical Society and the Institute of High Energy Physics of the Chinese Academy of Sciences and the Institute of Modern Physics of the Chinese Academy of Sciences and IOP Publishing Ltd

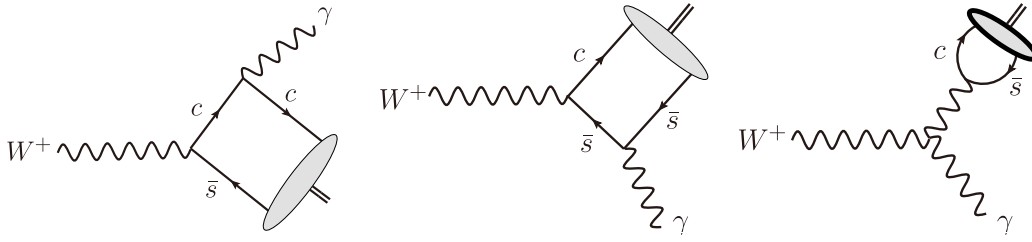


Fig. 1. Tree-level Feynman diagrams for the decay $W^+ \rightarrow D_s^+ \gamma$.

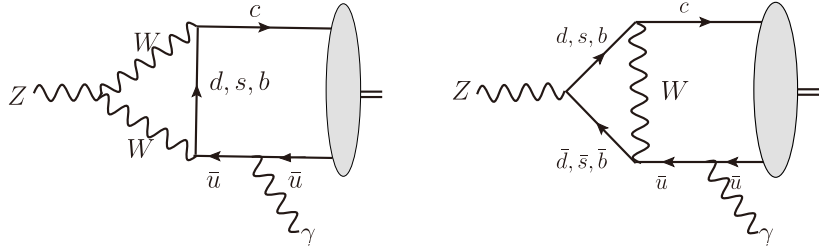


Fig. 2. Feynman diagrams contributing to the $Z \rightarrow D^0 \gamma$ decay in the SM.

II. DETECTOR AND SIMULATION

The LHCb detector [14, 15] is a single-arm forward spectrometer covering the pseudorapidity range $2 < \eta < 5$, designed for the study of particles containing b or c quarks. The detector includes a high-precision tracking system consisting of a silicon-strip vertex detector surrounding the pp interaction region [16], a large-area silicon-strip detector located upstream of a dipole magnet with a bending power of about 4 Tm, and three stations of silicon-strip detectors and straw drift tubes [17, 18] placed downstream of the magnet. The tracking system provides a measurement of the momentum, p , of charged particles with a relative uncertainty that varies from 0.5% at low momentum to 1.0% at 200 GeV/ c . The minimum distance of a track to a primary pp collision vertex (PV), the impact parameter (IP) [15], is measured with a resolution of $(15 + 29/p_T) \mu\text{m}$, where p_T is the component of the momentum transverse to the beam, in GeV/ c . Different types of charged hadrons are distinguished using information from two ring-imaging Cherenkov detectors [19]. Photons, electrons and hadrons are identified by a calorimeter system consisting of scintillating-pad and preshower detectors, an electromagnetic and a hadronic calorimeter [15, 20]. Charged and neutral clusters in the electromagnetic calorimeter are discerned by extrapolating the tracks reconstructed by the tracking system to the calorimeter plane. Photon and neutral pions are distinguished by cluster shape and energy distribution. The read-out electronics of the electromagnetic calorimeter is optimised for the typical energy deposits that occur in LHCb, *i.e.* heavy flavour physics, which results in a maximum detectable transverse energy of 10 GeV. A photon with very high energy is expected to have at least one sat-

urated calorimeter cell. Photons and neutral pions are distinguished by cluster shape, energy and mass distributions. Muons are identified by a system composed of alternating layers of iron and multiwire proportional chambers [21].

The online event selection is performed by a trigger, which consists of a hardware stage followed by a two-level software stage. In between the two software stages, an alignment and calibration of the detector is performed in near real-time and their results are used in the trigger [22]. The same alignment and calibration information is propagated to the offline reconstruction, ensuring a consistent and high quality reconstruction and event selection between the trigger and offline software. The identical performance of the online and offline reconstruction offers the opportunity to perform physics analyses directly using candidates reconstructed in the trigger [23, 24], which the present analysis exploits to reduce the event size by one order of magnitude.

Simulation is required to model the effects of the detector acceptance and the imposed selection requirements. In the simulation, pp collisions are generated using Pythia [25] with a specific LHCb configuration [26]. Decays of unstable particles are described by EvtGen [27], in which final-state radiation is generated using Photos [28]. The interaction of the generated particles with the detector, and its response, are implemented using the Geant4 toolkit [29] as described in Ref. [30]. In the signal simulation, the decay probability of $D_s^+ \rightarrow K^+ K^- \pi^+$ is taken to be uniform across the available phase space. However, there are sizable resonance contributions in the D_s^+ decay, which are accounted for by assigning weights to the simulated candidates. The weights are evaluated by

comparing the Dalitz distribution of the D_s^+ decay [31] and a phase-space model at the generator level.

III. RECONSTRUCTION AND SELECTION

The $W^+ \rightarrow D_s^+ (\rightarrow K^+ K^- \pi^+) \gamma$ and $Z \rightarrow D^0 (\rightarrow K^- \pi^+) \gamma$ candidates must be matched to a positive decision in the hardware trigger, which selects events by exploiting the particular signature of a photon with a high-energy cluster in the electromagnetic calorimeter and hadrons with high-transverse-energy deposits, E_T , in the calorimeters.

In the first software trigger stage, the charged final-state particles are required to be inconsistent with originating from a PV, and are further required to pass a boosted decision tree (BDT) multivariate selector [32], where the input variables rely on transverse momentum, vertex fit quality, and flight distance information for D_s^+ and D^0 candidates. In the second software trigger stage, $D_s^+ \rightarrow K^+ K^- \pi^+$ candidates are reconstructed from three tracks each with $p_T > 0.25$ GeV/ c . To further suppress background, additional requirements are applied to the combination of tracks, by requiring at least one of the three tracks to have p_T greater than 1.0 GeV/ c , at least two of them to have p_T greater than 0.4 GeV/ c , and the scalar p_T sum of the three tracks to be greater than 3 GeV/ c . The D_s^+ candidate is required to have a reconstructed invariant mass in the range [1.879, 2.059] GeV/ c^2 , and $p_T > 15$ GeV/ c . The D_s^+ candidate is further required to have a good vertex fit quality, and the D_s^+ vertex is required to be displaced from every PV by a distance corresponding to a D_s^+ decay time larger than 0.2ps. An additional neutral particle, which must be identified as a photon and have E_T greater than 10 GeV, is then combined with the D_s^+ candidate to form a $W^+ \rightarrow D_s^+ (\rightarrow K^+ K^- \pi^+) \gamma$ candidate. The W candidate must have invariant mass between 30 and 130 GeV/ c^2 . Similarly, $D^0 \rightarrow K^- \pi^+$ candidates are reconstructed from two tracks that pass track quality requirements, with $p_T > 0.5$ GeV/ c and $p > 5$ GeV/ c . The D^0 candidate is required to have reconstructed mass in the range [1.715, 2.015] GeV/ c^2 , and p_T greater than 15 GeV/ c . The D^0 candidate must have a good vertex fit quality and must be displaced from every PV. Each $Z \rightarrow D^0 (\rightarrow K^- \pi^+) \gamma$ candidate is reconstructed from a D^0 candidate plus a photon with $E_T > 10$ GeV. The Z boson candidates are required to have the invariant mass between 30 and 130 GeV/ c^2 .

In the offline selection, the photon candidates are required to satisfy $E_T > 15$ GeV. Background due to photons from π^0 decays is rejected by a dedicated algorithm [33]. The final-state particles associated with the $D_s^+ \rightarrow K^+ K^- \pi^+$ candidates are further required to have p_T greater than 0.5 GeV/ c and be located within the LHCb fiducial region. Two opposite-charged tracks are required to be identified as kaon tracks. The D_s^+ mass re-

gion is restricted to the range [1.92, 2.02] GeV/ c^2 , while the $D_s^+ p_T$ is required to be greater than 20 GeV/ c . A similar offline selection is applied to the $D^0 \rightarrow K^- \pi^+$ candidates, with the D^0 mass window requirement fixed to [1.82, 1.92] GeV/ c^2 . Contamination from decays of other particles is suppressed by dedicated mass veto requirements. The decay $D^+ \rightarrow K^- \pi^+ \pi^+$, with a charged pion misidentified as a kaon, could contribute to the $D_s^+ \rightarrow K^+ K^- \pi^+$ decay. Similarly the decay $D^{*+} \rightarrow D^0 (\rightarrow K^+ K^-) \pi^+$ with the same final-state particles but different peak positions, could also contribute to the selected D_s^+ candidates. A mass veto requirement $|M(K^- \pi^+ \pi^+) - 1.870| > 0.02$ GeV/ c^2 is employed to reject the D^+ background. The background contribution from the D^{*+} process is removed with the condition $M(K^+ K^-) < 1.85$ GeV/ c^2 . The background contribution from $\Lambda_c^+ \rightarrow p K^- \pi^+$ decay is studied and found to be well described as part of the combinatorial background. In total, 41718 and 73554 candidates are selected for $W^+ \rightarrow D_s^+ \gamma$ and $Z \rightarrow D^0 \gamma$, respectively.

The event selection of the normalization channels is similar to that used in previous LHCb publications [34, 35]. The online event selection is performed with the single muon triggers. At the hardware trigger stage, events are required to include a muon with high p_T . The muon candidate must satisfy $p_T > 6$ GeV/ c , $p > 8$ GeV/ c , with a good track fit quality in the first software trigger stage. In the second software trigger stage, the muon candidate is further required to satisfy $p_T > 12.5$ GeV/ c . For a $W^+ \rightarrow \mu^+ \nu$ candidate, the muon is required to pass all three single-muon trigger decision stages, and for a $Z \rightarrow \mu^+ \mu^-$ candidate, at least one of the muons must pass all three decision stages.

The offline $W^+ \rightarrow \mu^+ \nu$ candidate selection starts by requiring events to have a well-reconstructed muon candidate [15, 36] with p_T between 20 and 70 GeV/ c and $2.0 < \eta < 4.5$. The relative uncertainty in the momentum measurement for the muon is required to be less than 10%. Different background contributions have been considered and specific selection conditions have been devised in order to suppress the various contributions. Since a muon from a W^+ boson decay is typically isolated from other particles, an isolation requirement is applied on the muon to suppress background contributions, where one muon is originating from a QCD process. To reduce the contamination from $Z \rightarrow \mu^+ \mu^-$ decays, events are required to have no additional muon candidate with p_T above 2 GeV/ c . Background contamination from $Z \rightarrow \tau^+ \tau^-$ and heavy-flavour events is suppressed by requiring the IP of the muon candidate to be smaller than 40 μm . Muons from W boson decay, which tend to be highly isolated, are associated with low energy deposits in the electromagnetic and hadronic calorimeters. Therefore, the amount of energy that is deposited in the calorimeters relative to the momentum of the track is required to be small-

ler than 4%, which reduces the background from energetic pions and kaons punching through the calorimeters to the muon stations. In total, 4.4 million $W^+ \rightarrow \mu^+\nu$ candidates are selected with a purity of about 78%.

For the $Z \rightarrow \mu^+\mu^-$ offline selection, the candidates are required to have a pair of well-reconstructed tracks of opposite charge identified as muons. Muon tracks must have a p_T greater than 20 GeV/c and $2.0 < \eta < 4.5$. The invariant mass of the two muons must be in the range of 60 to 120 GeV/c². The relative uncertainty in the momentum measurement for each muon is required to be less than 10%. In total, 320000 $Z \rightarrow \mu^+\mu^-$ candidates are selected with a purity of about 98.5%.

IV. YIELD DETERMINATION

To determine the yields of W^+ and Z candidates, the pseudomass is used. Similarly to the one used in Ref. [37], it is defined as

$$m(M\gamma) = \sqrt{2p^M p_T^M \frac{p^\gamma}{p_T^\gamma} (1 - \cos\theta)}, \quad (1)$$

where p^M and p_T^M are the momenta and transverse momenta of the meson, p^γ and p_T^γ are the momenta and transverse momenta of the photon, and θ is the opening angle between the meson and the photon. The pseudomass is an approximation of the invariant mass in which the photon energy, which is poorly measured for transverse energies above the saturation value, is cancelled, resulting in more than 5% improvement on the expected upper limit. The selected $W^+ \rightarrow D_s^+\gamma$ candidates with pseudomass between 35 and 120 GeV/c², and the selected $Z \rightarrow D^0\gamma$ candidates with pseudomass between 50 and 125 GeV/c² are used in the yield determination. An extended maximum-likelihood method is adopted, with the finite template statistics accounted for, according to Ref. [38]. Upper limits on the signal yields are determined with the CL_S method [39, 40], using the candidate pseudomass and p_T distributions, and their correlations. The upper limits are calculated at 95% confidence level (C.L.), with the asymptotic CL_S method in the RooStats framework [41, 42] taking into account systematic uncertainties.

The signal shapes are determined from simulation after event selection. The background shape is estimated using a background-dominated sample, following a data-driven method used previously by the ATLAS collaboration [11, 43]. The background-dominated data sample is selected using candidates in the meson invariant mass sideband, with the requirement on the meson p_T changed from 20 GeV/c to 15 GeV/c. Since the D^0 lower mass sideband region contains background contributions from partially reconstructed decays (such as $D_s^+ \rightarrow K^+K^-\pi^+$

with a missing K^+ and $D^0 \rightarrow K^+\pi^+\pi^0$ with a missing π^0), the upper sideband region is selected [1.91, 2.00] GeV/c² for the $Z \rightarrow D^0\gamma$ background study. For D_s^+ candidates, both lower [1.90, 1.94] GeV/c² and upper [2.00, 2.05] GeV/c² sideband regions are used. Probability density functions (PDFs) are used to model the distributions of the selected background events, and correlations between different variables are taken into account using Gaussian kernel density estimation (KDE) [44]. Pseudodata candidates are generated, from which the background shape in the discriminating variable is derived. The ensemble of pseudodata candidates is produced by randomly sampling distributions of the relevant kinematic variables. These candidates are described by meson and photon four-momentum vectors:

- The meson four-momentum vector is constructed from its pseudorapidity (η_M), azimuthal angle (ϕ_M), mass (m_M), and transverse momentum (p_T^M).
- For the photon four-momentum vector, the p_T^γ of the selected photon candidate is used, while the photon pseudorapidity, η_γ , and azimuthal angle, ϕ_γ , are determined from the sampled $\Delta\eta(M, \gamma)$ and $\Delta\phi(M, \gamma)$ values, where $\Delta\eta(M, \gamma)$ and $\Delta\phi(M, \gamma)$ are the differences in η and ϕ between the meson and the photon.

The correlations among these kinematic variables in background events are retained in the generation of the pseudodata through the following sampling scheme:

- The η_M , ϕ_M , m_M , and p_T^M values are drawn randomly and independently according to the corresponding PDFs using the meson sideband data events. In the background-dominated data samples, the correlations between these variables are found to be negligible, therefore the variables are assumed to be uncorrelated.
- The distributions of p_T^γ , $\Delta\phi(M, \gamma)$ and $\Delta\eta(M, \gamma)$ are parameterised in bins of p_T^M , and values are drawn from the distributions of the bin corresponding to the previously generated p_T^M value.

Pseudodata candidates that pass the standard selection are used to construct two-dimensional template distributions of pseudomass and p_T .

The distributions of pseudomass and p_T for the signal candidates, overlaid with the signal and background models, are shown in Fig. 3. With no visible signal contribution, upper limits on the relative and absolute branching fractions are calculated.

V. RATIO OF BRANCHING FRACTIONS

The ratio $\mathcal{R}(W)$ of the $W^+ \rightarrow D_s^+\gamma$ branching fraction

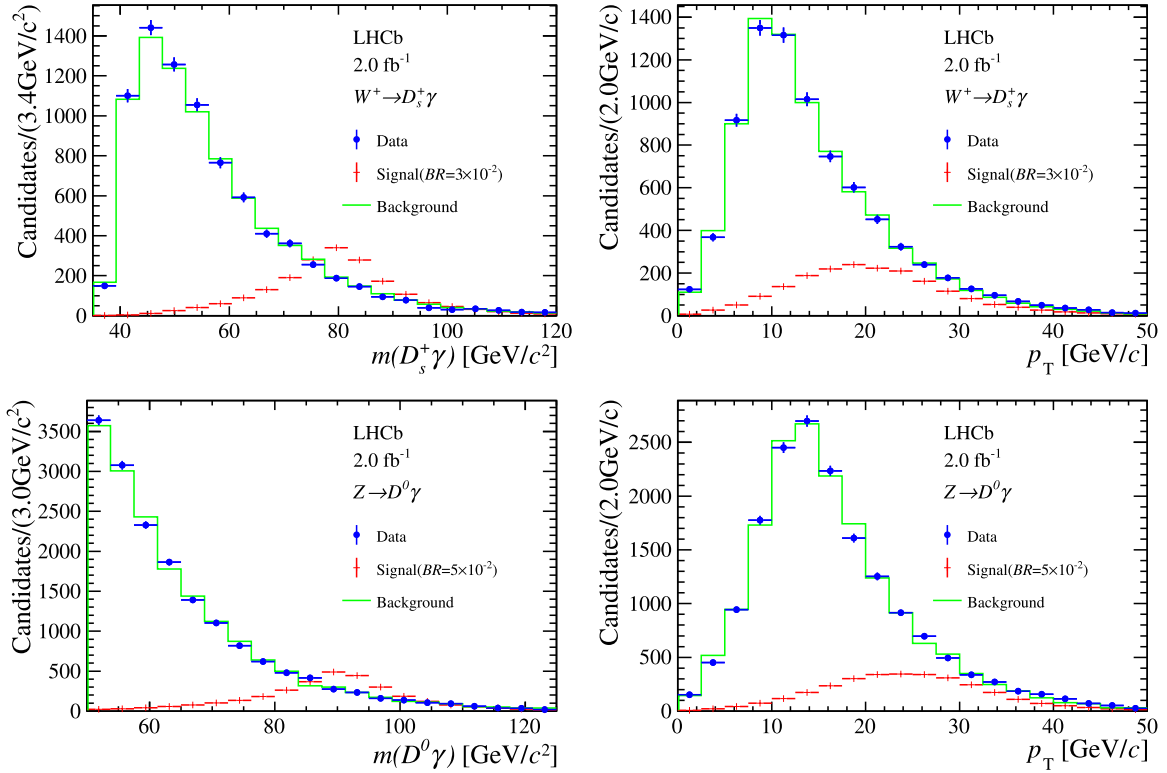


Fig. 3. (color online) Distributions of (left) pseudomass and (right) p_T for (upper) $W^+ \rightarrow D_s^+ \gamma$ and (lower) $Z \rightarrow D^0 \gamma$ candidates. The blue points represent the selected data candidates, the red points represent simulated signal events, normalized to the branching fraction of $W^+ \rightarrow D_s^+ \gamma$ ($Z \rightarrow D^0 \gamma$) set to 3×10^{-2} (5×10^{-2}), and the green lines represent the background shape, derived from pseudodata.

relative to that of the $W^+ \rightarrow \mu^+ \nu$ decay is defined as

$$\mathcal{R}(W) \equiv \frac{\mathcal{B}(W^+ \rightarrow D_s^+ \gamma)}{\mathcal{B}(W^+ \rightarrow \mu^+ \nu)} = \frac{N_s \times \varepsilon_n \times \mathcal{A}_n}{N_n \times \varepsilon_s \times \mathcal{A}_s} \times \frac{1}{\mathcal{B}(D_s^+ \rightarrow K^+ K^- \pi^+)}, \quad (2)$$

where $\mathcal{B}(W^+ \rightarrow D_s^+ \gamma)$ is the branching fraction of $W^+ \rightarrow D_s^+ \gamma$ decay, $\mathcal{B}(W^+ \rightarrow \mu^+ \nu)$ is the branching fraction of $W^+ \rightarrow \mu^+ \nu$ decay, and $\mathcal{B}(D_s^+ \rightarrow K^+ K^- \pi^+)$ is the branching fraction of $D_s^+ \rightarrow K^+ K^- \pi^+$ process; N_s (N_n) is the total signal (normalization) yield after event selection and background subtraction; \mathcal{A}_s (\mathcal{A}_n) is the probability for the true W boson decay charged products momenta to lie within the LHCb acceptance, ε_s (ε_n) is the total trigger, reconstruction and selection efficiency of the signal (normalization) channel.

The equivalent ratio of branching fractions, $\mathcal{R}(Z)$, and absolute branching fraction of the $Z \rightarrow D^0 \gamma$ decay are studied using the $Z \rightarrow \mu^+ \mu^-$ decay as a normalization channel. With the requirement that the final-state particle must be in the LHCb detector fiducial region, the definition can be written as

$$\mathcal{R}(Z) \equiv \frac{\mathcal{B}(Z \rightarrow D^0 \gamma)}{\mathcal{B}(Z \rightarrow \mu^+ \mu^-)} = \frac{N_s \times \varepsilon_n \times \mathcal{A}_n}{N_n \times \varepsilon_s \times \mathcal{A}_s} \times \frac{1}{\mathcal{B}(D^0 \rightarrow K^- \pi^+)}, \quad (3)$$

where $\mathcal{B}(Z \rightarrow D^0 \gamma)$ is the branching fraction of $Z \rightarrow D^0 \gamma$ decay, $\mathcal{B}(Z \rightarrow \mu^+ \mu^-)$ is the branching fraction of $Z \rightarrow \mu^+ \mu^-$ decay, and $\mathcal{B}(D^0 \rightarrow K^- \pi^+)$ is the branching fraction of $D^0 \rightarrow K^- \pi^+$ process.

As the number of final-state particles is different between signal and normalization channels, the acceptance correction is determined and applied to the \mathcal{R} calculation. The \mathcal{A}_s and \mathcal{A}_n factors are evaluated using event generators. In the acceptance study, the uncertainty from parton distribution functions is taken as a systematic uncertainty. The efficiencies ε_s and ε_n are determined from control and simulated samples. For signal, the event selection efficiencies are determined from simulation, where the track detection and particle identification efficiencies are calibrated with the data [45–47]. The photon identification efficiency is calibrated using a $B^0 \rightarrow K^{*0} \gamma$ control sample which is widely tested and used for the calibration of photon variables inside the LHCb collaboration, using only events with a photon of $E_T > 10$ GeV. The muon efficiencies are estimated using $Z \rightarrow \mu^+ \mu^-$ data candidates with the tag-and-probe method [35].

VI. SYSTEMATIC UNCERTAINTIES

The systematic uncertainties in the $\mathcal{R}(W)$ and $\mathcal{R}(Z)$ measurements are summarised in Table 1. The uncertainties in the $D_s^+ \rightarrow K^+ K^- \pi^+$ and $D^0 \rightarrow K^- \pi^+$ branching fractions are 1.86% and 0.76%, respectively [48]. The uncertainties of the normalization modes are expected to be uncorrelated with the uncertainties of the signal modes. Systematic uncertainties from normalization channels are studied separately for the $W^+ \rightarrow \mu^+ \nu$ and $Z \rightarrow \mu^+ \mu^-$ channels. Uncertainties from background estimation, efficiency calculations, signal determination and limited simulation sample size are taken into account, leading to relative uncertainties of 0.96% for $Z \rightarrow \mu^+ \mu^-$ and 3.08% for $W^+ \rightarrow \mu^+ \nu$ decays in the $\mathcal{R}(W)$ and $\mathcal{R}(Z)$ measurements. The $W^+ \rightarrow D_s^+ \gamma$ simulation is corrected using the measured Dalitz-plot distribution. To determine the uncertainty from the meson decay modelling, the binning width of the reference Dalitz-plot distribution is varied by a factor of 0.75.

An uncertainty is assigned due to the limited size of the simulation samples used to determine the event selection efficiency. The PID efficiency is calibrated using a control data sample [20], and a systematic uncertainty arises due to the limited sample size. The uncertainty is estimated by enlarging or decreasing the binning of p , η , and event multiplicity of the control sample by a factor of two. Similarly, the systematic uncertainty associated with the photon identification efficiency calibration is evaluated by varying the binning of the $B^0 \rightarrow K^{*0} \gamma$ control sample. The modelling of saturated calorimeter cells in the simulation is calibrated using $B^0 \rightarrow K^{*0} \gamma$ data events, and the systematic uncertainties from the size of the con-

trol sample and the binning schemes are studied. The combined uncertainty is determined to be 3.0% (3.1%) for $Z \rightarrow D^0 \gamma$ ($W^+ \rightarrow D_s^+ \gamma$). The uncertainty on the acceptance correction takes into account the size of the simulation samples, and uncertainties in the parton distribution function, factorisation and renormalisation scale dependencies as well as the uncertainty on α_s , combined in quadrature.

To estimate the systematic uncertainty from the background modelling, two sources are studied. The meson mass sideband regions are shifted to higher and lower masses by 0.03 GeV/ c^2 , and the deviations are assigned as uncertainty. An additional uncertainty is assigned by changing the binning of the meson p_T (by a factor of up to 50%) in the nonparametric data-driven approach, using finer and coarser binnings. The uncertainty from background modelling is determined to be 0.08% (0.36%) for the $Z \rightarrow D^0 \gamma$ ($W^+ \rightarrow D_s^+ \gamma$) search. The PV association algorithm was updated during the data-taking period, which causes a mismatch between LHCb data and simulation, and introduces systematic effects in the efficiency estimation. A correction is studied and applied to the simulation, and an uncertainty is assigned for this correction. An additional correction is applied to the simulation to account for imperfect modelling of the resolution of the meson invariant mass, by applying a 0.5% (0.6%) smearing correction to the D_s^+ (D^0) simulation. A systematic uncertainty is evaluated by varying the resolution correction within its statistical uncertainty.

VII. RESULTS

No significant peaking structure is found in the inspected pseudomass ranges. The CL_S method [39, 40] is used to calculate upper limits on the branching fractions of the $W^+ \rightarrow D_s^+ \gamma$ and $Z \rightarrow D^0 \gamma$ decays. In the calculation, we use the pseudomass and p_T distribution of W^+/Z boson candidates as observables, the signal shape is taken from the simulation after event selection, and the background distribution is estimated using a data-driven method. The upper limit on the ratios of branching fractions are determined to be

$$\mathcal{R}(Z) < 6.4 \times 10^{-2} \text{ at 95\% C.L.},$$

$$\mathcal{R}(W) < 6.1 \times 10^{-3} \text{ at 95\% C.L.}$$

The calculated and expected CL_S exclusions are shown as a function of the branching fraction for $W^+ \rightarrow D_s^+ \gamma$ and $Z \rightarrow D^0 \gamma$ decays in Fig. 4. The upper limits on the $W^+ \rightarrow D_s^+ \gamma$ and $Z \rightarrow D^0 \gamma$ rare decay branching fractions are determined to be

Table 1. Relative systematic uncertainties (in %) in the \mathcal{R} measurements for the $Z \rightarrow D^0 \gamma$ and $W^+ \rightarrow D_s^+ \gamma$ decay modes. The total systematic uncertainty is obtained from the sum in quadrature of all contributions.

Source	$Z \rightarrow D^0 \gamma$ (%)	$W^+ \rightarrow D_s^+ \gamma$ (%)
Meson BF	0.76	1.86
Normalization	0.96	3.08
Dalitz	–	0.24
MC sample size	0.11	0.09
PID	0.09	0.17
Photon ID	2.32	0.95
Calorimeter saturation	3.00	3.10
Background	0.08	0.36
Acceptance	0.57	0.82
PV association	0.57	0.29
Resolution	0.20	0.09
Total	4.07	4.94

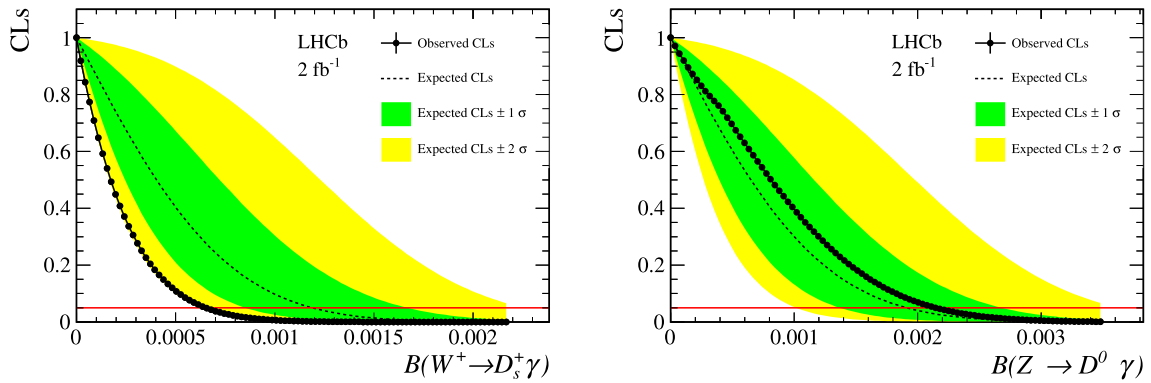


Fig. 4. (color online) Upper limits on branching fractions of the (left) $W^+ \rightarrow D_s^+ \gamma$ and (right) $Z \rightarrow D^0 \gamma$ decays.

$$\mathcal{B}(Z \rightarrow D^0 \gamma) < 2.1 \times 10^{-3} \text{ at 95\% C.L. ,}$$

$$\mathcal{B}(W^+ \rightarrow D_s^+ \gamma) < 6.5 \times 10^{-4} \text{ at 95\% C.L. ,}$$

using the known values [48] of the $Z \rightarrow \mu^+ \mu^-$ and $W^+ \rightarrow \mu^+ \nu$ branching ratios. The expected upper limit on the branching fraction is calculated to be 1.2×10^{-3} (1.9×10^{-3}) for the $W^+ \rightarrow D_s^+ \gamma$ ($Z \rightarrow D^0 \gamma$) decay.

VIII. CONCLUSION

Searches for the decays $W^+ \rightarrow D_s^+ \gamma$ and $Z \rightarrow D^0 \gamma$ are performed using pp collision data at $\sqrt{s} = 13$ TeV collected by the LHCb experiment in 2018, corresponding to an integrated luminosity of 2.0 fb^{-1} . No significant signal is observed above background. For the $W^+ \rightarrow D_s^+ \gamma$ decay, the upper limit is determined to be 6.5×10^{-4} at 95% C.L., which is the best limit to date. The first search for the decay $Z \rightarrow D^0 \gamma$ is performed, and the upper limit is determined to be 2.1×10^{-3} at 95% C.L. These limits are well above the range of their SM predictions. The next upgrade of the LHCb detector [49] will allow operation at a much higher instantaneous luminosity ($2 \times 10^{34} \text{ cm}^{-2} \text{ s}^{-1}$), while keeping good performance in reconstructing and identifying hadrons of different species. This upgrade will be well-suited for further study of these very rare decays of the W and Z bosons.

ACKNOWLEDGEMENTS













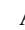

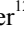





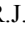
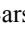



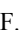



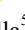
We express our gratitude to our colleagues in the

CERN accelerator departments for the excellent performance of the LHC. We thank the technical and administrative staff at the LHCb institutes. We are indebted to the communities behind the multiple open-source software packages on which we depend. We acknowledge support from CERN and from the national agencies: CAPES, CNPq, FAPERJ and FINEP (Brazil); MOST and NSFC (China); CNRS/IN2P3 (France); BMBF, DFG and MPG (Germany); INFN (Italy); NWO (Netherlands); MNiSW and NCN (Poland); MEN/IFA (Romania); MICINN (Spain); SNSF and SER (Switzerland); NASU (Ukraine); STFC (United Kingdom); DOE NP and NSF (USA). We acknowledge the computing resources that are provided by CERN, IN2P3 (France), KIT and DESY (Germany), INFN (Italy), SURF (Netherlands), PIC (Spain), GridPP (United Kingdom), CSCS (Switzerland), IFIN-HH (Romania), CBPF (Brazil), Polish WLCG (Poland) and NERSC (USA). Individual groups or members have received support from ARC and ARDC (Australia); Minciencias (Colombia); AvH Foundation (Germany); EPLANET, Marie Skłodowska-Curie Actions and ERC (European Union); A*MIDEX, ANR, IPhU and Labex P2IO, and Région Auvergne-Rhône-Alpes (France); Key Research Program of Frontier Sciences of CAS, CAS PIFI, CAS CCEPP, Fundamental Research Funds for the Central Universities, and Sci. & Tech. Program of Guangzhou (China); GVA, XuntaGal, GENCAT and Prog. Atracción Talento, CM (Spain); SRC (Sweden); the Leverhulme Trust, the Royal Society and UKRI (United Kingdom).

References

- [1] B. Guberina, J. H. Kuhn, R. D. Peccei *et al.*, *Nucl. Phys. B* **174**, 317 (1980)
- [2] N. N. Achasov, *Theor. Math. Phys.* **170**, 39 (2012)
- [3] T.-C. Huang and F. Petriello, *Phys. Rev. D* **92**, 014007 (2015), arXiv:1411.5924
- [4] L. Arnellos, W. J. Marciano, and Z. Parsa, *Nucl. Phys. B* **196**, 378 (1982)
- [5] Y. Grossman, M. König, and M. Neubert, *JHEP* **04**, 101 (2015), arXiv:1501.06569
- [6] A. V. Manohar, *Phys. Lett. B* **244**, 101 (1990)
- [7] G. Aad *et al.* (ATLAS collaboration), *Phys. Rev. Lett.* **114**, 121801 (2015), arXiv:1501.03276
- [8] M. Aaboud *et al.* (ATLAS collaboration), *Phys. Rev. Lett.*

- 117**, 111802 (2016), arXiv:1607.03400
- [9] M. Aaboud *et al.* (ATLAS collaboration), *JHEP* **07**, 127 (2018), arXiv:1712.02758
- [10] M. Aaboud *et al.* (ATLAS collaboration), *Phys. Lett. B* **786**, 134 (2018), arXiv:1807.00802
- [11] ATLAS collaboration, *Searches for exclusive Higgs and Z boson decays into a vector quarkonium state and a photon using 139 fb⁻¹ of ATLAS $\sqrt{s} = 13$ TeV proton-proton collision data*, arXiv:2208.03122
- [12] A. M. Sirunyan *et al.* (CMS collaboration), *Eur. Phys. J. C* **79**, 94 (2019), arXiv:1810.10056
- [13] F. Abe *et al.* (CDF collaboration), *Phys. Rev. D* **58**, 091101 (1998)
- [14] A. A. Alves Jr. *et al.* (LHCb collaboration), *JINST* **3**, S08005 (2008)
- [15] R. Aaij *et al.* (LHCb collaboration), *Int. J. Mod. Phys. A* **30**, 1530022 (2015), arXiv:1412.6352
- [16] R. Aaij *et al.*, *JINST* **9**, P09007 (2014), arXiv:1405.7808
- [17] R. Arink *et al.*, *JINST* **9**, P01002 (2014), arXiv:1311.3893
- [18] P. d'Argent *et al.*, *JINST* **12**, P11016 (2017), arXiv:1708.00819
- [19] M. Adinolfi *et al.*, *Eur. Phys. J. C* **73**, 2431 (2013), arXiv:1211.6759
- [20] C. Abellan Beteta *et al.*, *Calibration and performance of the LHCb calorimeters in Run 1 and 2 at the LHC*, arXiv:2008.11556, submitted to JINST.
- [21] A. A. Alves Jr. *et al.*, *JINST* **8**, P02022 (2013), arXiv:1211.1346
- [22] G. Dujany and B. Storaci, *J. Phys. Conf. Ser.* **664**, 082010 (2015)
- [23] R. Aaij *et al.*, *JINST* **8**, P04022 (2013), arXiv:1211.3055
- [24] R. Aaij *et al.*, *Comput. Phys. Commun.* **208**, 35 (2016), arXiv:1604.05596
- [25] T. Sjöstrand and S. Mrenna, *Comput. Phys. Commun.* **178**, 852 (2008), arXiv:0710.3820
- [26] I. Belyaev *et al.*, *J. Phys. Conf. Ser.* **331**, 032047 (2011)
- [27] D. J. Lange, *Nucl. Instrum. Meth. A* **462**, 152 (2001)
- [28] N. Davidson, T. Przedzinski, and Z. Was, *Comp. Phys. Comm.* **199**, 86 (2016), arXiv:1011.0937
- [29] J. Allison *et al.* (Geant4 Collaboration), *Geant4 Developments and Applications*, *IEEE Trans. Nucl. Sci.* **53**, 270 (2006); S. Agostinelli *et al.* (Geant4 Collaboration), *Geant4: A Simulation Toolkit*, *Nucl. Instrum. Meth. A* **506**, 250 (2003)
- [30] M. Clemencic *et al.*, *J. Phys. Conf. Ser.* **331**, 032023 (2011)
- [31] R. Aaij *et al.* (LHCb collaboration), *JHEP* **03**, 126 (2019), arXiv:1810.03138
- [32] V. V. Gligorov and M. Williams, *JINST* **8**, P02013 (2013), arXiv:1210.6861
- [33] M. Calvo Gomez *et al.*, *A tool for γ/π^0 separation at high energies*, CERN-LHCb-PUB-2015-016, 2015
- [34] R. Aaij *et al.* (LHCb collaboration), *JHEP* **01**, 155 (2016), arXiv:1511.08039
- [35] R. Aaij *et al.* (LHCb collaboration), *JHEP* **07**, 026 (2022), arXiv:2112.07458
- [36] F. Archilli *et al.*, *Journal of Instrumentation* **8**, P10020 (2013)
- [37] W. Barter, M. Pili, and M. Vesterinen, *Eur. Phys. J. C* **81** (2021)
- [38] R. J. Barlow and C. Beeston, *Comput. Phys. Commun.* **77**, 219 (1993)
- [39] A. L. Read, *J. Phys. G:Nucl. Part. Phys.* **28**, 2693 (2002)
- [40] T. Junk, *Confidence level computation for combining searches with small statistics*, *Nuclear Instruments and Methods in Physics Research Section A: Accelerators, Spectrometers, Detectors and Associated Equipment* **434**, 435 (1999)
- [41] L. Moneta *et al.*, *The RooStats project*, *PoS ACAT2010*, 057 (2010), arXiv:1009.1003
- [42] G. Cowan, K. Cranmer, E. Gross *et al.*, *Eur. Phys. J. C* **71**, 1554 (2011), arXiv:1007.1727
- [43] A. Chisholm *et al.*, *JHEP* **10**, 001 (2022), arXiv:2112.00650
- [44] K. S. Cranmer, *Comput. Phys. Commun.* **136**, 198 (2001), arXiv:hep-ex/0011057
- [45] R. Aaij *et al.* (LHCb collaboration), *JINST* **10**, P02007 (2015), arXiv:1408.1251
- [46] L. Anderlini *et al.*, *The PIDCalib package*, LHCb-PUB-2016-021, 2016
- [47] R. Aaij *et al.*, *Eur. Phys. J. Tech. Instr.* **6**, 1 (2019), arXiv:1803.00824
- [48] R. L. Workman (Particle Data Group), *PTEP* **2022**, 083C01 (2022)
- [49] LHCb collaboration, *Expression of Interest for a Phase-II LHCb Upgrade: Opportunities in flavour physics, and beyond, in the HL-LHC era*, CERN-LHCC-2017-003, 2017

R. Aaij³²  A.S.W. Abdelmotteleb⁵⁰  C. Abellan Beteta⁴⁴ F. Abudinén⁵⁰  T. Ackernley⁵⁴  B. Adeva⁴⁰ 
M. Adinolfi⁴⁸  P. Adlarson⁷⁷  H. Afsharnia⁹ C. Agapopoulou¹³  C.A. Aidala⁷⁸  Z. Ajaltouni⁹ S. Akar⁵⁹ 
K. Akiba³²  J. Albrecht¹⁵  F. Alessio⁴²  M. Alexander⁵³  A. Alfonso Albero³⁹  Z. Aliouche⁵⁶ 
P. Alvarez Cartelle⁴⁹  R. Amalric¹³  S. Amato²  J.L. Amey⁴⁸  Y. Amhis^{11,42}  L. An⁴²  L. Anderlini²² 
M. Andersson⁴⁴  A. Andreianov³⁸  M. Andreotti²¹  D. Andreou⁶²  D. Ao⁶  F. Archilli¹⁷ 
A. Artamonov³⁸  M. Artuso⁶²  E. Aslanides¹⁰  M. Atzeni⁴⁴  B. Audurier¹²  S. Bachmann¹⁷ 
M. Bachmayer⁴³  J.J. Back⁵⁰  A. Bailly-reyre¹³ P. Baladron Rodriguez⁴⁰  V. Balagura¹²  W. Baldini²¹ 
J. Baptista de Souza Leite¹  M. Barbetti^{22j}  R.J. Barlow⁵⁶  S. Barsuk¹¹  W. Barter⁵⁵  M. Bartolini⁴⁹ 
F. Baryshnikov³⁸  J.M. Basels¹⁴  G. Bassi^{29,p}  B. Batsukh⁴  A. Battig¹⁵  A. Bay⁴³  A. Beck⁵⁰ 
M. Becker¹⁵  F. Bedeschi²⁹  I.B. Bediaga¹  A. Beiter⁶²  V. Belavin³⁸  S. Belin⁴⁰  V. Bellee⁴⁴ 
K. Belous³⁸  I. Belov³⁸  I. Belyaev³⁸  G. Benane¹⁰  G. Bencivenni²³  E. Ben-Haim¹³ 
A. Berezhnoy³⁸  R. Bernet⁴⁴  S. Bernet Andres⁷⁶  D. Berninghoff¹⁷  H.C. Bernstein⁶²  C. Bertella⁵⁶ 

L.A. Granado Cardoso⁴² E. Graugés³⁹ E. Graverini⁴³ G. Graziani¹⁰ A. T. Grecu³⁷ L.M. Greeven³²
 N.A. Grieser⁴ L. Grillo⁵³ S. Gromov³⁸ B.R. Gruberg Cazon⁵⁷ C. Gu³ M. Guarise^{21,i}
 M. Guittiere¹¹ P. A. Günther¹⁷ E. Gushchin³⁸ A. Guth¹⁴ Y. Guz³⁸ T. Gys⁴² T. Hadavizadeh⁶³
 C. Hadjivasiliou⁶⁰ G. Haefeli⁴³ C. Haen⁴² J. Haimberger⁴² S.C. Haines⁴⁹ T. Halewood-leagas⁵⁴
 M.M. Halvorsen⁴² P.M. Hamilton⁶⁰ J. Hammerich⁵⁴ Q. Han⁷ X. Han¹⁷ E.B. Hansen⁵⁶
 S. Hansmann-Menzemer¹⁷ L. Hao⁶ N. Harnew⁵⁷ T. Harrison⁵⁴ C. Hasse⁴² M. Hatch⁴² J. He^{6,c}
 K. Heijhoff³² C. Henderson⁵⁹ R.D.L. Henderson^{63,50} A.M. Hennequin⁵⁸ K. Hennessy⁵⁴ L. Henry⁴²
 J. Herd⁵⁵ J. Heuel¹⁴ A. Hicheur² D. Hill⁴³ M. Hilton⁵⁶ S.E. Hollitt¹⁵ J. Horswill⁵⁶
 R. Hou⁷ Y. Hou⁸ J. Hu¹⁷ J. Hu⁶⁶ W. Hu⁵ X. Hu³ W. Huang⁶ X. Huang⁶⁸ W. Hulsbergen³²
 R.J. Hunter⁵⁰ M. Hushchyn³⁸ D. Hutchcroft⁵⁴ P. Ibis¹⁵ M. Idzik³⁴ D. Ilin³⁸ P. Ilten⁵⁹
 A. Inglessi³⁸ A. Iniukhin³⁸ A. Ishteev³⁸ K. Ivshin³⁸ R. Jacobsson⁴² H. Jage¹⁴ S.J. Jaimes Elles⁴¹
 S. Jakobsen⁴² E. Jans³² B.K. Jashal⁴¹ A. Jawahery⁶⁰ V. Jevtic¹⁵ E. Jiang⁶⁰ X. Jiang^{4,6}
 Y. Jiang⁶ M. John⁵⁷ D. Johnson⁵⁸ C.R. Jones⁴⁹ T.P. Jones⁵⁰ B. Jost⁴² N. Jurik⁴²
 I. Juszcak³⁵ S. Kandybei⁴⁵ Y. Kang³ M. Karacson⁴² D. Karpenkov³⁸ M. Karpov³⁸
 J.W. Kautz⁵⁹ F. Keizer⁴² D.M. Keller⁶² M. Kenzie⁵⁰ T. Ketel³² B. Khanji¹⁵ A. Kharisova³⁸
 S. Kholodenko³⁸ G. Khreich¹¹ T. Kim¹⁴ V.S. Kirsebom⁴³ O. Kitouni⁵⁸ S. Klaver³³
 N. Kleijne^{29,p} K. Klimaszewski³⁶ M.R. Kmiec³⁶ S. Koliiev⁴⁶ A. Kondybayeva³⁸
 A. Konoplyannikov³⁸ P. Kopciwicz³⁴ R. Kopečna¹⁷ P. Koppenburg³² M. Korolev³⁸ I. Kostiuk^{32,46}
 O. Kot⁴⁶ S. Kotriakhova¹⁰ A. Kozachuk³⁸ P. Kravchenko³⁸ L. Kravchuk³⁸ R.D. Krawczyk⁴²
 M. Krepš⁵⁰ S. Kretzschmar¹⁴ P. Krokovny³⁸ W. Krupa³⁴ W. Krzemien³⁶ J. Kubat¹⁷ S. Kubis⁷⁵
 W. Kucewicz^{35,34} M. Kucharczyk³⁵ V. Kudryavtsev³⁸ A. Kupsc⁷⁷ D. Lacarrere⁴² G. Lafferty⁵⁶
 A. Lai²⁷ A. Lampis^{27,h} D. Lancierini⁴⁴ C. Landesa Gomez⁴⁰ J.J. Lane⁵⁶ R. Lane⁴⁸
 G. Lanfranchi²³ C. Langenbruch¹⁴ J. Langer¹⁵ O. Lantwin³⁸ T. Latham⁵⁰ F. Lazzari^{29,t}
 M. Lazzaroni^{25,i} R. Le Gac¹⁰ S.H. Lee⁷⁸ R. Lefèvre⁹ A. Leflat³⁸ S. Legotin³⁸ P. Lenisa^{1,21}
 O. Leroy¹⁰ T. Lesiak³⁵ B. Leverington¹⁷ A. Li³ H. Li⁶⁶ K. Li⁷ P. Li¹⁷ P.-R. Li⁶⁷ S. Li⁷
 T. Li⁴ T. Li⁶⁶ Y. Li⁴ Z. Li⁶² X. Liang⁶² C. Lin⁶ T. Lin⁵¹ R. Lindner⁴²
 V. Lisovskyi¹⁵ R. Litvinov^{27,h} G. Liu⁶⁶ H. Liu⁶ Q. Liu⁶ S. Liu^{4,6} A. Lobo Salvia³⁹ A. Loi²⁷
 R. Lollini⁷² J. Lomba Castro⁴⁰ I. Longstaff⁵³ J.H. Lopes² A. Lopez Huertas³⁹ S. López Soliño⁴⁰
 G.H. Lovell⁴⁹ Y. Lu^{4,b} C. Lucarelli^{22,j} D. Lucchesi^{28,n} S. Luchuk³⁸ M. Lucio Martinez⁷⁴
 V. Lukashenko^{32,46} Y. Luo³ A. Lupato⁵⁶ E. Luppi^{21,i} A. Lusiani^{29,p} K. Lynch¹⁸ X.-R. Lyu⁶
 L. Ma⁴ R. Ma⁶ S. Maccolini²⁰ F. Machefert¹¹ F. Maciuc³⁷ I. Mackay⁵⁷ V. Macko⁴³
 P. Mackowiak¹⁵ L.R. Madhan Mohan⁴⁸ A. Maevskiy³⁸ D. Maisuzenko³⁸ M.W. Majewski³⁴
 J.J. Malczewski³⁵ S. Malde⁵⁷ B. Malecki^{35,42} A. Malinin³⁸ T. Maltsev³⁸ G. Manca^{27,h}
 G. Mancinelli¹⁰ C. Mancuso^{11,25,1} D. Manuzzi²⁰ C.A. Manzari⁴⁴ D. Marangotto^{25,1} J.F. Marchand⁸
 U. Marconi²⁰ S. Mariani^{22,j} C. Marin Benito³⁹ J. Marks¹⁷ A.M. Marshall⁴⁸ P.J. Marshall⁵⁴
 G. Martelli^{72,o} G. Martellotti³⁰ L. Martinazzoli^{1,42,m} M. Martinelli^{26,m} D. Martinez Santos⁴⁰
 F. Martinez Vidal⁴¹ A. Massafferri¹ M. Materok¹⁴ R. Matev⁴² A. Mathad⁴⁴ V. Matiunin³⁸
 C. Matteuzzi²⁶ K.R. Mattioli¹² A. Mauri³² E. Maurice¹² J. Mauricio³⁹ M. Mazurek⁴²
 M. McCann⁵⁵ L. McConnell¹⁸ T.H. McGrath⁵⁶ N.T. McHugh⁵³ A. McNab⁵⁶ R. McNulty¹⁸
 J.V. Mead⁵⁴ B. Meadows⁵⁹ G. Meier¹⁵ D. Melnychuk³⁶ S. Meloni^{26,m} M. Merk^{32,74} A. Merli^{25,1}
 L. Meyer Garcia² D. Miao^{4,6} M. Mikhasenko^{70,d} D.A. Milanese⁶⁹ E. Millard⁵⁰ M. Milovanovic⁴²
 M.-N. Minard^{8t} A. Minotti^{26,m} T. Miralles⁹ S.E. Mitchell⁵² B. Mitreska⁵⁶ D.S. Mitzel¹⁵
 A. Mödden¹⁵ R.A. Mohammed⁵⁷ R.D. Moise¹⁴ S. Mokhnenko³⁸ T. Mombächer⁴⁰ M. Monk^{50,63}
 I.A. Monroy⁶⁹ S. Monteil⁹ M. Morandin²⁸ G. Morello²³ M.J. Morello^{29,p} J. Moron³⁴
 A.B. Morris⁷⁰ A.G. Morris⁵⁰ R. Mountain⁶² H. Mu³ E. Muhammad⁵⁰ F. Muheim⁵²
 M. Mulder⁷³ K. Müller⁴⁴ C.H. Murphy⁵⁷ D. Murray⁵⁶ R. Murta⁵⁵ P. Muzzetto^{27,h} P. Naik⁴⁸

A. Valassi⁴²  G. Valenti²⁰  N. Valls Canudas⁷⁶  M. van Beuzekom³²  M. Van Dijk⁴³  H. Van Hecke⁶¹ 
E. van Herwijnen⁵⁵  C.B. Van Hulse^{40,v}  M. van Veghel⁷³  R. Vazquez Gomez³⁹  P. Vazquez Regueiro⁴⁰ 
C. Vázquez Sierra⁴²  S. Vecchi²¹  J.J. Velthuis⁴⁸  M. Veltri^{22,u}  A. Venkateswaran⁴³  M. Veronesi³² 
M. Vesterinen⁵⁰  D. Vieira⁵⁹  M. Vieites Diaz⁴³  X. Vilasis-Cardona⁷⁶  E. Vilella Figueras⁵⁴  A. Villa²⁰ 
P. Vincent¹³  F.C. Volle¹¹  D. vom Bruch¹⁰  A. Vorobyev³⁸  V. Vorobyev³⁸  N. Voropaev³⁸  K. Vos⁷⁴ 
C. Vrahas⁵²  R. Waldi¹⁷  J. Walsh²⁹  G. Wan⁵  C. Wang¹⁷  G. Wang⁷  J. Wang⁵  J. Wang⁴ 
J. Wang³  J. Wang⁶⁸  M. Wang²⁵  R. Wang⁴⁸  X. Wang⁶⁶  Y. Wang⁷  Z. Wang⁴⁴  Z. Wang³ 
Z. Wang⁶  J.A. Ward^{50,63}  N.K. Watson⁴⁷  D. Websdale⁵⁵  Y. Wei⁵  C. Weisser⁵⁸ 
B.D.C. Westhenry⁴⁸  D.J. White⁵⁶  M. Whitehead⁵³  A.R. Wiederhold⁵⁰  D. Wiedner¹⁵  G. Wilkinson⁵⁷ 
M.K. Wilkinson⁵⁹  I. Williams⁴⁹  M. Williams⁵⁸  M.R.J. Williams⁵²  R. Williams⁴⁹  F.F. Wilson⁵¹ 
W. Wislicki³⁶  M. Witek³⁵  L. Witola¹⁷  C.P. Wong⁶¹  G. Wormser¹¹  S.A. Wotton⁴⁹  H. Wu⁶² 
J. Wu⁷  K. Wyllie⁴²  Z. Xiang⁶  D. Xiao⁷  Y. Xie⁷  A. Xu⁵  J. Xu⁶  L. Xu³  L. Xu³ 
M. Xu⁵⁰  Q. Xu⁶  Z. Xu⁹  Z. Xu⁶  D. Yang³  S. Yang⁶  X. Yang⁵  Y. Yang⁶  Z. Yang⁵ 
Z. Yang⁶⁰  L.E. Yeomans⁵⁴  V. Yeroshenko¹¹  H. Yeung⁵⁶  H. Yin⁷  J. Yu⁶⁵  X. Yuan⁶² 
E. Zaffaroni⁴³  M. Zavertyaev¹⁶  M. Zdybal³⁵  O. Zenaiev⁴²  M. Zeng³  C. Zhang⁵  D. Zhang⁷ 
L. Zhang³  S. Zhang⁶⁵  S. Zhang⁵  Y. Zhang⁵  Y. Zhang⁵⁷  A. Zharkova³⁸  A. Zhelezov¹⁷ 
Y. Zheng⁶  T. Zhou⁵  X. Zhou⁶  Y. Zhou⁶  V. Zhovkovska¹¹  X. Zhu³  X. Zhu⁷  Z. Zhu⁶ 
V. Zhukov^{14,38}  Q. Zou^{4,6}  S. Zucchelli^{20,g}  D. Zuliani²⁸  G. Zunica⁵⁶ 

(LHCb Collaboration)

¹Centro Brasileiro de Pesquisas Físicas (CBPF), Rio de Janeiro, Brazil²Universidade Federal do Rio de Janeiro (UFRJ), Rio de Janeiro, Brazil³Center for High Energy Physics, Tsinghua University, Beijing, China⁴Institute Of High Energy Physics (IHEP), Beijing, China⁵School of Physics State Key Laboratory of Nuclear Physics and Technology, Peking University, Beijing, China⁶University of Chinese Academy of Sciences, Beijing, China⁷Institute of Particle Physics, Central China Normal University, Wuhan, China⁸Université Savoie Mont Blanc, CNRS, IN2P3-LAPP, Annecy, France⁹Université Clermont Auvergne, CNRS/IN2P3, LPC, Clermont-Ferrand, France¹⁰Aix Marseille Univ, CNRS/IN2P3, CPPM, Marseille, France¹¹Université Paris-Saclay, CNRS/IN2P3, IJCLab, Orsay, France¹²Laboratoire Leprince-Ringuet, CNRS/IN2P3, Ecole Polytechnique, Institut Polytechnique de Paris, Palaiseau, France¹³LPNHE, Sorbonne Université, Paris Diderot Sorbonne Paris Cité, CNRS/IN2P3, Paris, France¹⁴I. Physikalisches Institut, RWTH Aachen University, Aachen, Germany¹⁵Fakultät Physik, Technische Universität Dortmund, Dortmund, Germany¹⁶Max-Planck-Institut für Kernphysik (MPIK), Heidelberg, Germany¹⁷Physikalisches Institut, Ruprecht-Karls-Universität Heidelberg, Heidelberg, Germany¹⁸School of Physics, University College Dublin, Dublin, Ireland¹⁹INFN Sezione di Bari, Bari, Italy²⁰INFN Sezione di Bologna, Bologna, Italy²¹INFN Sezione di Ferrara, Ferrara, Italy²²INFN Sezione di Firenze, Firenze, Italy²³INFN Laboratori Nazionali di Frascati, Frascati, Italy²⁴INFN Sezione di Genova, Genova, Italy²⁵INFN Sezione di Milano, Milano, Italy²⁶INFN Sezione di Milano-Bicocca, Milano, Italy²⁷INFN Sezione di Cagliari, Monserrato, Italy²⁸Università degli Studi di Padova, Università e INFN, Padova, Padova, Italy²⁹INFN Sezione di Pisa, Pisa, Italy³⁰INFN Sezione di Roma La Sapienza, Roma, Italy³¹INFN Sezione di Roma Tor Vergata, Roma, Italy³²Nikhef National Institute for Subatomic Physics, Amsterdam, Netherlands³³Nikhef National Institute for Subatomic Physics and VU University Amsterdam, Amsterdam, Netherlands³⁴AGH - University of Science and Technology, Faculty of Physics and Applied Computer Science, Kraków, Poland³⁵Henryk Niewodniczanski Institute of Nuclear Physics Polish Academy of Sciences, Kraków, Poland³⁶National Center for Nuclear Research (NCBJ), Warsaw, Poland³⁷Horia Hulubei National Institute of Physics and Nuclear Engineering, Bucharest-Magurele, Romania

- ³⁸Affiliated with an institute covered by a cooperation agreement with CERN
³⁹ICCUB, Universitat de Barcelona, Barcelona, Spain
⁴⁰Instituto Galego de Física de Altas Enerxías (IGFAE), Universidade de Santiago de Compostela, Santiago de Compostela, Spain
⁴¹Instituto de Física Corpuscular, Centro Mixto Universidad de Valencia - CSIC, Valencia, Spain
⁴²European Organization for Nuclear Research (CERN), Geneva, Switzerland
⁴³Institute of Physics, Ecole Polytechnique Fédérale de Lausanne (EPFL), Lausanne, Switzerland
⁴⁴Physik-Institut, Universität Zürich, Zürich, Switzerland
⁴⁵NSC Kharkiv Institute of Physics and Technology (NSC KIPT), Kharkiv, Ukraine
⁴⁶Institute for Nuclear Research of the National Academy of Sciences (KINR), Kyiv, Ukraine
⁴⁷University of Birmingham, Birmingham, United Kingdom
⁴⁸H.H. Wills Physics Laboratory, University of Bristol, Bristol, United Kingdom
⁴⁹Cavendish Laboratory, University of Cambridge, Cambridge, United Kingdom
⁵⁰Department of Physics, University of Warwick, Coventry, United Kingdom
⁵¹STFC Rutherford Appleton Laboratory, Didcot, United Kingdom
⁵²School of Physics and Astronomy, University of Edinburgh, Edinburgh, United Kingdom
⁵³School of Physics and Astronomy, University of Glasgow, Glasgow, United Kingdom
⁵⁴Oliver Lodge Laboratory, University of Liverpool, Liverpool, United Kingdom
⁵⁵Imperial College London, London, United Kingdom
⁵⁶Department of Physics and Astronomy, University of Manchester, Manchester, United Kingdom
⁵⁷Department of Physics, University of Oxford, Oxford, United Kingdom
⁵⁸Massachusetts Institute of Technology, Cambridge, MA, United States
⁵⁹University of Cincinnati, Cincinnati, OH, United States
⁶⁰University of Maryland, College Park, MD, United States
⁶¹Los Alamos National Laboratory (LANL), Los Alamos, NM, United States
⁶²Syracuse University, Syracuse, NY, United States
⁶³School of Physics and Astronomy, Monash University, Melbourne, Australia, associated to ⁵⁰
⁶⁴Pontificia Universidade Católica do Rio de Janeiro (PUC-Rio), Rio de Janeiro, Brazil, associated to ²
⁶⁵Physics and Micro Electronic College, Hunan University, Changsha City, China, associated to ⁷
⁶⁶Guangdong Provincial Key Laboratory of Nuclear Science, Guangdong-Hong Kong Joint Laboratory of Quantum Matter, Institute of Quantum Matter, South China Normal University, Guangzhou, China, associated to ³
⁶⁷Lanzhou University, Lanzhou, China, associated to ⁴
⁶⁸School of Physics and Technology, Wuhan University, Wuhan, China, associated to ³
⁶⁹Departamento de Física, Universidad Nacional de Colombia, Bogota, Colombia, associated to ¹³
⁷⁰Universität Bonn - Helmholtz-Institut für Strahlen und Kernphysik, Bonn, Germany, associated to ¹⁷
⁷¹Eotvos Lorand University, Budapest, Hungary, associated to ⁴²
⁷²INFN Sezione di Perugia, Perugia, Italy, associated to ²¹
⁷³Van Swinderen Institute, University of Groningen, Groningen, Netherlands, associated to ³²
⁷⁴Universiteit Maastricht, Maastricht, Netherlands, associated to ³²
⁷⁵Tadeusz Kosciuszko Cracow University of Technology, Cracow, Poland, associated to ³⁵
⁷⁶DS4DS, La Salle, Universitat Ramon Llull, Barcelona, Spain, associated to ³⁹
⁷⁷Department of Physics and Astronomy, Uppsala University, Uppsala, Sweden, associated to ⁵³
⁷⁸University of Michigan, Ann Arbor, MI, United States, associated to ⁶²
^aUniversidade de Brasília, Brasília, Brazil
^bCentral South U., Changsha, China
^cHangzhou Institute for Advanced Study, UCAS, Hangzhou, China
^dExcellence Cluster ORIGINS, Munich, Germany
^eUniversidad Nacional Autónoma de Honduras, Tegucigalpa, Honduras
^fUniversità di Bari, Bari, Italy
^gUniversità di Bologna, Bologna, Italy
^hUniversità di Cagliari, Cagliari, Italy
ⁱUniversità di Ferrara, Ferrara, Italy
^jUniversità di Firenze, Firenze, Italy
^kUniversità di Genova, Genova, Italy
^lUniversità degli Studi di Milano, Milano, Italy
^mUniversità di Milano Bicocca, Milano, Italy
ⁿUniversità di Padova, Padova, Italy
^oUniversità di Perugia, Perugia, Italy
^pScuola Normale Superiore, Pisa, Italy
^qUniversità di Pisa, Pisa, Italy
^rUniversità della Basilicata, Potenza, Italy
^sUniversità di Roma Tor Vergata, Roma, Italy
^tUniversità di Siena, Siena, Italy
^uUniversità di Urbino, Urbino, Italy
^vUniversidad de Alcalá, Alcalá de Henares, Spain

†Deceased